ADVANCED QUANTUM TECHNOLOGIES
www.advquantumtech.com

# Solid-State Quantum Emitters

*A. Mark Fox*

**This perspective gives a tutorial overview of the development of solid-state quantum emitters over the past three decades, focusing on the key parameters that are used to assess their performance for applications in quantum photonics. Specifically, it covers single-photon purity and indistinguishability, source brightness, and on-demand operation. The perspective includes a brief comparison of different material systems and concludes with a discussion of challenges that remain to be solved.**

## 1. Introduction

A "quantum emitter" is a source that emits light with properties that cannot be explained by classical theories. The hall-mark of such a source is the observation of photon anti-bunching, which was first observed in 1977 by Kimble, Dagenais, and Mandel in a resonance fluorescence experiment on a beam of sodium atoms.[1] The key technical step that enabled the breakthrough was the ability to collect the photons emitted by just a single atom within the atomic beam.

The first generation of experiments that followed ref. [1] mainly focused on gaseous systems, and it took about 15 years for the ideas to be transferred to the solid state. The strategy for observing quantum effects involved isolating single emitters, which effectively act like individual "solid-state atoms". In this way, anti-bunching was observed for single molecules embedded within a crystal in 1992,[2] and then for individual color centers and semiconductor quantum dots in 2000.[3,4]

In the years that followed these first experiments, quantum emitters have been observed in a great variety of solid-state materials, and the performance of the sources has improved dramatically. In this perspective, I give an overview of the key parameters that characterize quantum emitters when using them as single-photon sources. I also discuss challenges and opportunities that have emerged as the field has developed and new material systems have become available. The aim is not to give a comprehensive review of the present state-of-the-art, but rather to identify benchmarks and discuss key points that have to be addressed as new materials come to the fore.

A. M. Fox
Department of Physics & Astronomy
University of Sheffield
Sheffield S3 7RH, UK
E-mail: mark.fox@sheffield.ac.uk

The ORCID identification number(s) for the author(s) of this article can be found under https://doi.org/10.1002/qute.202300390



**DOI: 10.1002/qute.202300390**

## 2. Characterization of Quantum Emitters

In this section, four factors that affect the performance of quantum emitters are discussed, namely: single-photon purity, photon indistinguishability, source brightness, and on-demand operation. These topics have been previously considered in a number of detailed review articles (see, for example,[5,6]) and the discussion given here only covers basic concepts that are important for the rest of the perspective. A discussion of different types of materials is given in Section 3, with a comparison of their relative pros and cons in Section 4.

### 2.1. Single-Photon Purity

The principal parameter that characterizes a quantum emitter is the value of the second-order correlation function $g^{(2)}(\tau)$ at $\tau = 0$. An ideal quantum emitter has $g^{(2)}(0) = 0$ and its value is measured in a Hanbury Brown–Twiss (HBT) experiment. The first experiment of this type was performed in 1956 to explore the properties of light emitted by a mercury lamp,[7] and the results enabled the classical second-order correlation function of the 435.8 nm line to be measured. It took more than 20 years to improve the experiments by developing better detectors and learning how to isolate photons from single emitters to the point that quantum-optical effects could be observed.

**Figure 1** gives a schematic diagram of an HBT experiment. The light is split by a 50:50 beam splitter and registered by two separate single-photon detectors. The detectors are connected to a timer, which is started when a click is registered on one of the detectors (e.g., D1). The timer then waits until another photon from the stream is split toward the other detector (e.g., D2) and generates the stop click. The results are displayed as histograms giving the number of time-binned events versus $\tau$, the time between detector clicks. The histograms that emerge from these experiments are directly related to $g^{(2)}(\tau)$ through:

$$g^{(2)}(\tau) = CN(\tau) \tag{1}$$

where $C$ is a normalization constant and $N(\tau)$ is the number of events where a click on detector D2 occurred at a time $t + \tau$ after a click on D1 at time $t$. Negative $\tau$ implies that the click on D2 occurred before the one on D1. The normalization constant is found by setting the value of $g^{(2)}(\tau)$ equal to 1 for $\tau \to \infty$. This assumes that there are no correlations between the arrival

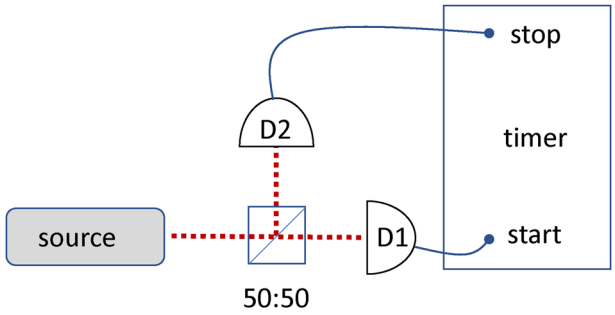


**Figure 1.** Schematic of a Hanbury Brown–Twiss (HBT) experiment. D1 and D2 are single-photon detectors.

times of the photons at very long times, making all time separations equally likely. In practice, this requires that $g^{(2)}(\tau)$ is measured out to values of $\tau$ longer than all the internal timescales of the emitter. As a minimum, we require measurements out to $|\tau| \gg \tau_r$, where $\tau_r$ is the radiative lifetime. However, care needs to be taken, as there can sometimes be effects occurring on much slower timescales (e.g., blinking) that can lead to errors in determining $C$ correctly.[8]

The basic principle that underlies quantum emitters is to isolate a single emitter, as in the atomic-beam experiment of Kimble et al. in 1977.[1] The emitter is promoted to an excited state, and then decays through a series of optical transitions of different frequencies. If we isolate a single emitter, there can only be one photon emitted for each transition, and we therefore obtain only one photon of a particular frequency each time the atom is excited. This photon can be selected by placing a filter in the collection path, as illustrated in **Figure 2a**. In order to emit another photon of the same wavelength, the atom must be excited again, and follow the same decay path. Since the excitation and emission process takes a minimum time of $\tau_r$ (the radiative lifetime), the probability of emitting two photons of the same wavelength at the same time is very small at short time differences. This gives rise to a dip in $N(\tau)$ at $\tau = 0$ as shown in Figure 2b, with the width of the dip determined by the radiative emission time. This dip is a signature of photon anti-bunching, which is a purely quantum-optical effect that is not compatible with classical theories of light.

Figure 2c illustrates the HBT results expected for a quantum emitter when excited by a pulsed laser. A classical source would emit pulses separated by $T$, where $1/T$ is the excitation rate. Clicks can be observed on the detectors at times separated by integer multiples of $T$ giving rise to peaks in $N(\tau)$ with a width determined by the pulse width, which is itself governed by $\tau_r$. The hallmark of the quantum emitter is the absence of the peak at $\tau = 0$, showing that the pulses contain only one photon and hence cannot give rise to coincidences at the same time.

The value of $g^{(2)}(0)$ measured in an HBT experiment is the first parameter used to compare quantum emitters. Any source with $g^{(2)}(0) < 1$ qualifies as a quantum emitter, since classical emitters always have $g^{(2)}(0) \geq 1$. (See e.g..[9]) Similarly, a source that has $g^{(2)}(0) < 0.5$ qualifies as a single-photon emitter, since two-photon sources give $g^{(2)}(0) = 0.5$. However, for most applications, we want $g^{(2)}(0)$ to be as close to zero as possible. Reasons that can contribute to a value of $g^{(2)}(0) > 0$ include:

1. difficulties in isolating single emitters;
2. difficulties in selecting single transitions;
3. refilling of the emitter by carriers from the surrounding, e.g., by nearby traps after the first photon has been emitted.
4. inadequate detector response times;
5. classical background emission.

The results of Kimble et al. in 1977[1] gave $g^{(2)}(0) \approx 0.4$ and were limited by the first problem, namely the difficulty of observing photons from just a single atom within an atomic beam. The second problem arises when the emitter decays by a cascade of transitions with similar frequencies, as can be the case for quantum dots. The third problem is a risk for all solid-state systems, and drives research into purer materials. The fourth is a measurement artefact, and does not necessarily reflect badly on the emitter: the anti-bunching dip cannot be resolved if the detector response time is larger than $\tau_r$, and this issue becomes more serious for the best emitters with very fast radiative lifetimes. This will not normally be a problem now that efficient superconducting single-photon detectors are available that have response times of $\approx$ 20 ps. The final problem is especially relevant to solid-state systems, where the quantum emitter is embedded within a host crystal that can sometime generate classical light at the same wavelength as the quantum emitter. If all these problems are overcome, nearly ideal performance can be observed, with $g^{(2)}(0) < 10^{-4}$ measured in the best cases.[10]

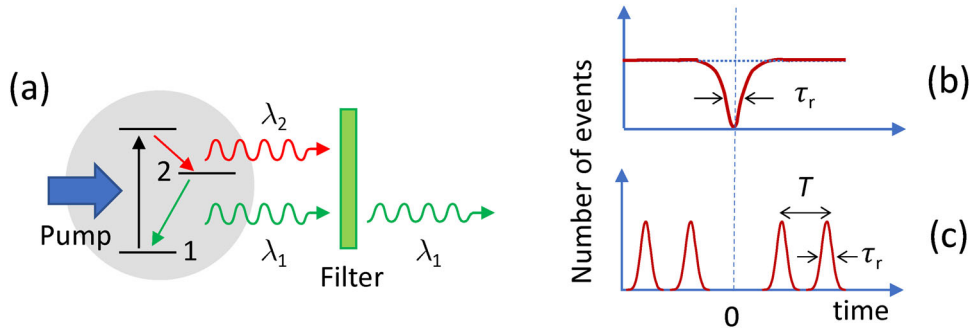


**Figure 2.** a) Excitation of a single atom producing a single photon on a specific transition. In this case, the photon emitted by the 2 → 1 transition is selected after filtering. b) Idealized histogram of the time-dependence of the number of events recorded in an HBT experiment on a quantum emitter under CW excitation, using detectors with a response time much faster than the radiative lifetime, $\tau_r$, of the emitter. c) Equivalent results for pulsed excitation with pulse rate $1/T$.

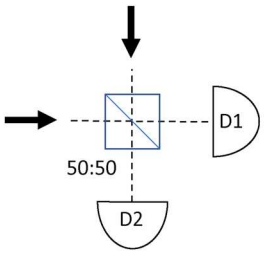


| Outcomes | Distinguishable | Indistinguishable |
|---|---|---|
| Both to D1 | 25 % | 50 % |
| One to D1, other to D2 | 50 % | 0 |
| Both to D2 | 25 % | 50 % |

**Figure 3.** Schematic depiction of a Hong–Ou–Mandel experiment. The table gives the probabilities for the possible outcomes when single photons enter the beam splitter via the two input ports.

### 2.2. Photon Indistinguishability

Some applications in quantum photonics (e.g., linear optics quantum computation) require that the photons should be indistinguishable from each other. The degree of indistinguishability is measured by performing Hong–Ou–Mandel (HOM) experiments,[11] where two photons impinge on separate input ports of a 50:50 beam splitter, with detectors D1 and D2 positioned at the output ports, as shown in **Figure 3**. There are three possible outcomes: both photons go to detector D1, both go to D2, or one goes to D1 and the other to D2. The table in Figure 3 gives the probabilities for these three outcomes for two extreme cases. If the photons are completely distinguishable, they both exit the beam splitter with 50% probability of going either to D1 or to D2. This gives a 50% probability of coincidence events where both detectors click. On the other hand, if the photons are completely indistinguishable, the path amplitudes interfere, and the probability of observing coincidences drops to zero. The degree of photon indistinguishability $\mathcal{V}$ can therefore be determined by measuring the drop in coincidence events in a HOM experiment, with $\mathcal{V} = 1$ implying that the photons are totally indistinguishable.

High photon indistinguishability is only obtained when dephasing processes are eliminated, since the interaction between the emitter and the environment provides, in principle, a memory in the system that time-tags a specific photon. Hence $\mathcal{V}$ is limited by the coherence, and is given by:

$$\mathcal{V} = \frac{T_2}{2T_1} \tag{2}$$

where $T_2$ and $T_1$ are related to each other through:

$$\frac{1}{T_2} = \frac{1}{2T_1} + \frac{1}{T_2^*} \tag{3}$$

Here, $T_2$ is the coherence time, $T_1$ is the population decay time, and $T_2^*$ is the dephasing time. $T_2$ can be measured with a Michelson interferometer, while $T_1$ can be measured by time-resolved photoluminescence. The ideal scenario is where the only decay channel is radiative, so that $T_1 = \tau_r$, and the dephasing rate $1/T_2^*$ is negligible. In this situation, called the Fourier limit, $T_2 = 2\tau_r$ and $\mathcal{V} = 1$.

The challenge in solid-state systems is to control the environment of the emitter so that dephasing processes occur on a much slower timescale than the radiative emission. For some emitters, the uncontrolled charges associated either with non-resonant excitation or with defects cause dephasing by generating random electric fields that perturb the emitter via the Stark effect. These effects can be eliminated by embedding the emitter in a diode that controls its electrical environment and using resonant excitation to prevent generation of unwanted free carriers in the device.[12] Phonon scattering, however, is always an issue in solid-state materials, and the sources generally only have high coherence when operated at low temperatures. An effective approach to mitigating against dephasing is to speed up the radiative emission using the Purcell effect (see Section 2.3) to the point that $1/T_2^*$ is negligible compared to $1/2\tau_R$.

### 2.3. Brightness

The brightness of a quantum emitter is affected by many factors and is not defined in the same way by different authors, causing ambiguity in the literature. The National Institute of Standards and Technology (NIST) in the United States has recently produced an internal report attempting to clarify the relevant definitions.[13] In this Section I focus on two key factors that affect the brightness, namely the speed at which photons can be emitted and the efficiency with which they can be collected and detected. In the next Section I discuss techniques for true on-demand operation, which also affects the brightness by ensuring that the source emits a photon with probability approaching 100% for each clock cycle.

The maximum photon emission rate is governed by its radiative lifetime $\tau_r$. There is a great variation in $\tau_r$ between different types of emitters, ranging from nanoseconds to milliseconds. The 589 nm transition of sodium used in ref. [1]) has a lifetime of 16 ns, implying maximum photon emission rates of $\approx 10^8\,s^{-1}$. The lifetimes of some solid-state quantum emitters (e.g., molecules, quantum dots) can be faster on account of their larger physical size, giving larger dipole moments. However, other types of emitters can be slower if the transitions are electric-dipole forbidden (e.g., rare-earth ions: see Section 3.7).

The transition rate is governed by the photon density of states, which is proportional to $\nu^2$ in a uniform dielectric, where $\nu$ is the frequency. All other things being equal, this implies that the radiative lifetime increases with increasing wavelength. For example, the typical radiative lifetime of InAs quantum dots increases from about 1 ns at $\approx$ 900 nm[14] to closer to 2 ns at 1550 nm.[15] However, the lifetime is not completely fixed, as the density of states can be engineered using optical cavities. The

Purcell factor $F_P$ that determines the radiative enhancement in the cavity compared to the bulk is given by (see e.g.,[9]):

$$F_P = \frac{W_{21}^{cavity}}{W_{21}^{bulk}} = \frac{\tau_r}{\tau_r^{cavity}} = \frac{3Q(\lambda/n)^3}{4\pi^2 V}\,\xi^2\,\frac{\Delta\nu_c^2}{4(\nu-\nu_c)^2+\Delta\nu_c^2} \tag{4}$$

where $Q$ is the quality factor, $V$ is the mode volume, $\lambda = c/\nu$ is the vacuum wavelength, $n$ is the refractive index of the cavity material, $\nu_c$ is the cavity frequency, and $\Delta\nu_c = \nu_c/Q$ is the spectral width of the mode. The factor $\xi$ is the normalized dipole orientation factor defined by:

$$\xi = \frac{|\boldsymbol{p}\cdot\boldsymbol{E}|}{|\boldsymbol{p}||\boldsymbol{E}|} \tag{5}$$

where \boldmath $p$ is the dipole moment of the emitter and \boldmath $E$ is the field-profile of the cavity. $\xi$ is equal to unity when the dipole is aligned with the polarization of the cavity and is positioned at the maximum of the field. In the ideal scenario when the emitter is exactly in resonance with the cavity (i.e. $\nu = \nu_c$) and $\xi = 1$, the Purcell factor reduces to:

$$F_P = \frac{3Q(\lambda/n)^3}{4\pi^2 V} \tag{6}$$

This implies that we can obtain enhanced emission (i.e., shorter radiative lifetime) for high-$Q$ cavities with small modal volumes with dimensions comparable to the wavelength inside the crystal.

Purcell's original work in 1946 considered the emission from atoms and molecules within microwave cavities that had ≈ cm dimensions commensurate with the optical wavelength.[16] The ability to make high-$Q$ cavities with ≈ 1 μm dimensions and smaller, as required for optical frequencies, has only become a reality with the development of nano-fabrication techniques such as electron-beam lithography. This is a key strength of solid-state emitters, especially those based in semiconducting host crystals, since they are compatible with advanced processing technologies.

The prospect of enhancing the emission rate in the cavity encourages intense research efforts to develop micro- and nano-cavities with very small modal volumes and high quality factors, building on pioneering work demonstrating a shortened lifetime for quantum dots coupled to a micro-pillar cavity in 1998.[14] In this way, it has been shown that the radiative lifetime of an InAs quantum dot can be reduced from ≈ 1 ns in the bulk to ≈ 20 ps by using a photonic-crystal nanocavity.[17] The much larger Purcell factor in ref. [17] compared to the earlier work is related to the smaller modal volume of the photonic-crystal nanocavity compared to the micro-pillar, and also to the use of resonant excitation techniques that by-pass internal relaxation processes that can limit the emission speed.

It should be pointed out that the maximum Purcell enhancement is only achieved when the emitter is tuned to resonance with the cavity and positioned with maximal overlap with the cavity field, as shown by Equation (4). Tuning to resonance was originally done by varying the temperature, with the emitter frequency shifting faster than the cavity mode, but the more recent results have typically used Stark tuning, exploiting the ability to fabricate diode structures with the emitters in regions with voltage-controllable DC electric fields. (See e.g., ref. [17] or [18]) The requirement of optimal positioning is not so straight-forward for solid-state emitters that are located at random positions within a crystal, and it is usually necessary to fabricate many devices and search for one with an emitter at the right position. In the long run, it is more efficient to register the position of the emitter first and then to fabricate the cavity around it. (See e.g.,[19] and further discussion in Section 4.)

The internal quantum efficiency of the emitter is another factor that must be considered. There might be several decay paths from the excited state, so that a particular transition would only be obtained according to a branching ratio. This problem can be removed by using resonant excitation methods, where the emitter is promoted directly to the upper level of the transition. Another potential problem is that the emitter jumps randomly between bright states that emit photons and dark states that do not, or shifts in and out of resonance with an exciting laser due to spectral wandering. This produces an intermittent stream of photons, an effect known as blinking.[20] These blinking effects can be minimized by controlling the environment of the emitter.

The brightness of a source is also determined by the photon collection efficiency.[21] Emitters in uniform dielectrics emit over the whole $4\pi$ solid angle, which makes it impossible to collect all the photons using a single lens. Moreover, with solid-state systems there is the additional problem that the emitter is embedded within a host crystal that has a high refractive index, which means that most of the photons are trapped within the crystal by total-internal reflection. Cavities can help here too, as the photons are preferentially emitted into the cavity mode rather than into $4\pi$ solid angle, as in the bulk, and can thus funnel the photons into the collection optics. The parameter of interest is the $\beta$-factor that quantifies the fraction of photons emitted into the mode. This is clearly related to the Purcell factor since the latter determines the emission rate to the cavity mode. In fact, the two parameters are related to each other, with:

$$\beta = \frac{F_P}{1+F_P} \tag{7}$$

Hence a large Purcell factor gives a large $\beta$-factor approaching the optimal value of unity. By designing cavities with asymmetric end-mirror reflectivities, so that photons can be coupled out preferentially on one side, and using the Purcell effect to enhance the $\beta$-factor, the collection efficiency can be greatly enhanced compared to the bulk, thus overcoming the photon collection problem. In this way, coupling efficiencies into an optical fibre approaching unity have been achieved.[22]

### 2.4. On-Demand Operation

An ideal quantum emitter behaves as a deterministic single-photon source that emits exactly one photon on-demand in response to a pump pulse. This contrasts with probabilistic single-photon sources based on heralded down-conversion and attenuated lasers, which rely on the low probability for multi-photon emission when $\overline{n}$, the average photon number per pulse, is small, i.e. $\overline{n} \ll 1$. This is an inevitable consequence of the underlying Poissonian photon statistics of these sources, and forces them to operate with $\overline{n} \approx 0.1$, which means that a particular time bin

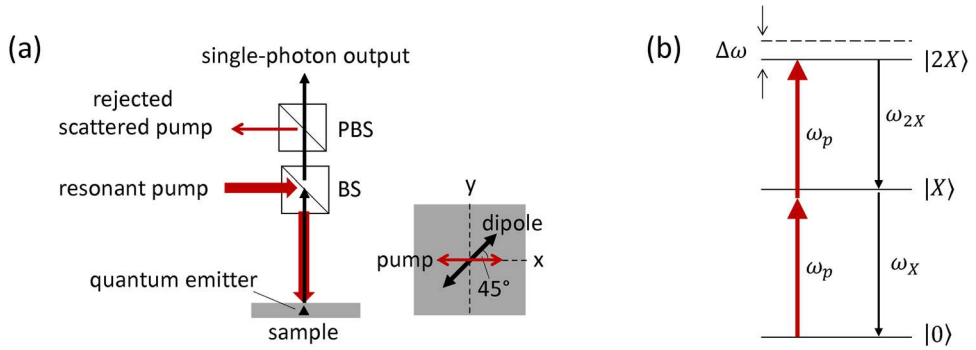


**Figure 4.** a) Schematic of a pumping scheme for collecting resonance fluorescence from a quantum emitter. An *x*-polarized pump laser is fed to the sample via a non-polarizing beam splitter (BS) with a small reflection and high transmission coefficient. Scattered pump light and the single photons pass through BS toward a polarizing beam splitter (PBS) that rejects the pump. The sample is orientated with the emitter's dipole at 45° to the *x*-axis, so that the photons it emits can pass through the polarizer with 50% probability. b) Level scheme for two-photon pumping of the biexciton state. $\Delta\omega = (\omega_X - \omega_{2X})$ is the frequency splitting between the exciton $|X\rangle$ and biexciton $|2X\rangle$ transitions, and the pump frequency is set at the midpoint with $\omega_p = (\omega_X + \omega_{2X})/2$.

might contain a photon only with ≈ 10% probability. By contrast, an ideal on-demand source emits exactly one photon with 100% probability for each pulse, and solid-state quantum emitters can operate in this regime when coherent-control methods are used.

Coherent control techniques were first developed for nuclear magnetic resonance (NMR) experiments. The system is excited by an electromagnetic pulse that is resonant with the transition frequency and has a duration $T_{\text{pulse}}$ that is shorter than the coherence time $T_2$. NMR transitions typically occur in the radio-frequency (≈ MHz) range, and the coherence times of the nuclei involved are often in the μs range, or longer. This makes it relatively straightforward to satisfy the condition $T_{\text{pulse}} < T_2$. However, for solid-state quantum emitters operating at optical frequencies, we need to control the electrons, which have much shorter coherence times due, for example, to their strong interaction with phonons. This means that very short pulses in the picosecond or femtosecond range from ultrafast lasers have to be used.

The effect of an ultrashort resonant laser pulse in the coherent-control regime is determined by the Bloch-vector rotation angle Θ. For a laser pulse with a time-varying electric field amplitude $\mathcal{E}_0(t)$, the rotation angle is given by

$$\Theta = \int_{-\infty}^{+\infty} \Omega_R(t)\,\mathrm{d}t \tag{8}$$

where $\Omega_R(t)$ is the time-varying Rabi frequency:

$$\Omega_R(t) = \left|\frac{\mu_{12}\mathcal{E}_0(t)}{\hbar}\right| \tag{9}$$

with $\mu_{12}$ being the transition dipole moment. The case of a $\pi$-pulse where $\Theta = \pi$ is of special interest. These pulses deterministically promote the system from the ground state to the excited state, thus providing a method to generate a photon for every pulse excitation cycle. This deterministic state preparation is the preferred method for on-demand single-photon sources in which the system produces a photon in response to a trigger pulse with probability approaching 100%.

Despite the benefits, the use of resonant $\pi$-pulse excitation methods does present some technical challenges that make it difficult to implement in the field. The problem is that the photon that is emitted has the same frequency as the laser pulse, and hence has to be carefully separated. The standard way to do this is to use polarization optics. We pump using one polarization (e.g., *x*) and only collect light with the opposite polarization (i.e., y) with a polarizer in the collection path to block the scattered laser photons, as shown in **Figure 4a**. This works if the emitter dipole is orientated at 45° to the *x* and *y* axes, so that the driving field has a component parallel to the dipole, and the emitting dipole has a component along the collection polarization. The need to resolve the *x*-polarized pump laser along the 45° direction is not a problem, as we can just double the power to get the same pumping field, but the 45° orientation of the emitter dipole relative to the *y*-polarized collection path is an issue, as it means that we lose half the photons that are emitted.

An ingenious method to get around this problem is to use an elliptical cavity with two oppositely polarized cavity modes with slightly different frequencies.[23] The emitter is in resonance with the *y*-polarized cavity, which enhances the emission probability for *y*-polarized photons through the Purcell effect, and can be pumped via the off-resonance *x*-polarized cavity mode. The coupling of the laser through the off-resonant cavity mode is therefore relatively weak, but this is not a problem, as the laser power can simply be turned up. The key here is to pump the quantum emitter via the *x* mode, but all the photons are emitted into the *y* mode due to the Purcell effect, giving very high emission probability.

The need to separate the pump laser from the emitted photon has prompted research to develop methods in which the excitation frequency is not exactly resonant with the transition. A common approach is to pump the system to the biexciton state by two-photon excitation, as shown in Figure 4. The interaction between the excitons leads to a frequency splitting $\Delta\omega = \omega_X - \omega_{2X}$ between the exciton $|X\rangle$ and biexciton $|2X\rangle$ transitions, where $\hbar\Delta\omega$ is the biexciton binding energy. The two-photon transition occurs at $\omega_p = (\omega_X + \omega_{2X})/2$, and can easily be filtered out. This leads to high purity single-photon emission on both the exciton

and biexciton transitions, with $g^{(2)}(0) < 10^{-4}$ reported using this method (see e.g.,[10]). Other non-resonant approaches for deterministic population of the excited state include:

a) phonon sideband pumping, where $\omega_p = \omega_X + \Omega$, where $\hbar\Omega$ is the energy of an acoustic phonon, typically a few meV;[24,25]
b) dichromatic pumping with two pulses detuned symmetrically on either side of the exciton such that $\omega_1 = \omega_X + \Delta$ and $\omega_2 = \omega_X - \Delta$;[26]
c) dichromatic pumping by the SUPER method (Swing-UP of quantum EmitteR population), where both pulses are red-detuned from the transition.[27]

The price that is paid for using detuned pulses is that higher powers have to be used to invert the population. This is not an issue for proof-of-principle experiments, but could eventually become important for multi-emitter systems in which power budgets have to be considered. There could also be a trade-off between excitation power and $g^{(2)}(0)$, for example due to increasing background emission, leading to a reduction in the single-photon purity at the higher pump powers.

## 3. Quantum-Emitter Materials

### 3.1. Overview

The need for single-photon sources in photonic quantum technologies motivates research to improve established materials and to develop new ones.[28] In comparing different platforms, consideration has to be taken of the four features discussed in Section 2, namely: single-photon purity, photon indistinguishability, brightness, and on-demand operation. However, these are not the only factors that have to be considered, and two other important ones are the wavelength and the operating temperature.

The wavelength that is required is determined by the application. Emitters optimized for optical fibre systems are of particular interest. Short-range local area networks tend to operate in the near infrared spectral region around 900 nm, while long-range systems work in the telecom O-band (1260–1360 nm) and C-band (1530–1565 nm) wavelength ranges. Emitters that are optimized for spectral regions where atmospheric losses are low are also of particular interest for free-space quantum channels (e.g., to satellites). Visible quantum emitters can be used in this application, while near infrared wavelengths (e.g., C-band) benefit from lower atmospheric losses and reduced background from the Sun.[29]

Quantum emitters generally work best at cryogenic temperatures. This is acceptable for laboratory demonstrations, but wide-scale deployment will require operation at higher temperatures. The target is to achieve room temperature operation, but a compromise solution is to reach temperatures that are accessible with miniature cryocoolers.

In the subsections that follow, a brief survey of different material systems is given, with a summary in **Table 1**. More detailed performance indicators for some specific single-photon sources are given in **Table 2**. The table includes results at both cryogenic temperatures and room temperature, and the radiative lifetime $\tau_r$ is included, as this is the parameter that ultimately limits the count rate that can be achieved. Note that all the results in Table 2 for a specific source are obtained at the same time. This is an important consideration, as there is often a trade-off between performance parameters such as the single-photon purity and the detected count rate, with better values of $g^{(2)}(0)$ generally obtained at low excitation levels where the detected count rate is lower. Thus it might be possible to achieve world-best results for single-photon purity or indistinguishability at low powers, but the performance achieved when operating under $\pi$-pulse excitation or at saturation can be much worse.

### 3.2. Epitaxial Quantum Dots

At present, the best results for on-demand single-photon sources have been obtained using epitaxial semiconductor quantum dots (QDs). (See ref. [31] or [90] for reviews.) This is because of the availability of advanced semiconductor technology that enables growth of samples with very high purity and the fabrication of highly sophisticated nano-photonic devices.

Much of the work has focused on (In,Ga)As/GaAs devices that emit around 900 nm and have a radiative lifetime of about 1 ns. With resonant excitation techniques (see Section 2.4) it is possible to promote the QD to the upper level of the desired transition with near unity efficiency, leading to optimal on-demand operation, with values of $\mathcal{V}$ approaching unity.[91] The indistinguishability remains high for photons separated by long times compared to the pulse separation (13 ns), but eventually drops off on microsecond timescales due to spectral diffusion associated with charge fluctuations in the vicinity of the QD.[92] The charge state of the quantum dot can stabilized by embedding the QDs within diode structures with controlled gating. The depletion of the carriers reduces intermittency (i.e., blinking) associated with random charging and discharging of nearby traps,[93] and also leads to transform-limited linewidths.[12] Purcell enhancement of a very high quality gated quantum dot has facilitated negligible drop-off in the indistinguishability for photons emitted with $\approx 1\mu s$ time separation.[18] The photon collection problem has been overcome by embedding the QDs inside nano-cavities that funnel all the photons to a specific optical channel with high efficiency. The nano-cavity can also be used to speed up the emission via the Purcell effect, thereby improving the brightness. Very large Purcell factors are possible for small nano-cavities with high quality factors, and this has been shown to improve the coherence of a QD source to the Fourier limit even in devices with average electrical properties.[17]

By combining all of these techniques, the QDs approximate very well to ideal deterministic single-photon sources, surpassing all other rival technologies. (See e.g. refs. [18, 32–34]) The first row in Table 2 lists the results achieved in ref. [18], which represents the present state-of-the-art for an on-demand single-photon source excited by $\pi$-pulses in terms of end-to-end efficiency and detected count rate combined with very good single-photon purity and HOM visibility. Comparable results, albeit with lower end-to-end efficiency, have been reported for InGaAs/GaAs QD devices that are now available commercially and have been implemented in a single-photon-based quantum computing platform.[94]

The (In,Ga)As/GaAs sources emitting at about 900 nm are well suited for local-area networks, but longer wavelengths are needed at larger distances. The emission wavelength depends on

**Table 1.** Representative list of material systems for solid-state emitters and their emission wavelengths. The references give a flavor of some of the relevant recent work, or are review articles. The single-photon purity $g^{(2)}(0)$ is the best value reported in the references cited. More detailed performance indicators for some of the emitters are given in Table 2. UV: ultraviolet, NIR: near infrared; TMDC: transition-metal dichalcogenide.

| Material system | Material details | Wavelength range | $g^{(2)}(0)$ | References |
|---|---|---|---|---|
| Epitaxial quantum dots | (InGa)As/GaAs | 900 – 1300 nm | 0.000095 | [30–34] |
| | InAs/InP | telecom C-band | 0.0032 | [15, 35, 36] |
| | InAs/GaAs on metamorphic buffer | telecom C-band | 0.003 | [37, 38] |
| | GaAs/AlGaAs | ≈ 780 nm | 0.000075 | [10, 39] |
| | nitrides: GaN/AlN, InGaN/GaN | UV-visible | 0.05 | [31, 40, 41] |
| Colloidal quantum dots | II-VI semiconductor | visible, NIR | 0.01 | [42–44] |
| | InP | visible, NIR | 0.03 | [45, 46] |
| | perovskite | visible | 0.019 | [47, 48] |
| Molecular | polyaromatic hydrocarbons | visible, NIR | < 0.03 | [49–51] |
| | carbon nanotubes | telecom O-band | 0.02 | [52, 53] |
| Color centers | diamond: NV (nitrogen vacancy) | 637 nm | 0.21 | [54, 55] |
| | diamond: SiV (silicon vacancy) | 738 nm | 0.0168 | [56, 57] |
| | diamond: GeV (germanium vacancy) | 602 nm | 0.06 | [58–60] |
| | diamond: PbV (lead vacancy) | 552 nm | 0.2 | [61] |
| | diamond: SnV (tin vacancy) | 619 nm | 0.09 | [62, 63] |
| | silicon | 1100 – 1550 nm | 0.20 | [64, 65] |
| | silicon carbide | 1000 – 1400 nm | 0.05 | [66, 67] |
| | silicon nitride | 550 – 750 nm | 0.12 | [68] |
| | hexagonal boron nitride (hBN) | visible | 0.01 | [69, 70] |
| 2D materials | TMDCs: $WS_2$, $WSe_2$, $MoSe_2$ | NIR | 0.002 | [71–74] |
| | TMDCs: $MoTe_2$ | 1080 – 1550 nm | 0.058 | [75] |
| Rare earth ions | $Nd^{3+}$ | 880 nm | 0.09 | [76] |
| | $Yb^{3+}$ | 980 nm | 0.26 | [77–79] |
| | $Er^{3+}$ | 1550 nm | 0.018 | [80, 81] |

**Table 2.** Performance indicators for pulsed single-photon sources using solid-state quantum emitters. The results are all obtained under the same operating conditions unless stated otherwise. The count rate is the measured value without allowing for the imperfect detector efficiency. $g^{(2)}(0)$: HBT measurement, indicating the single-photon purity; $\tau_r$: radiative lifetime; $\mathcal{V}$: HOM visibility; QD: quantum dot; DBT: dibenzoterrylene single molecule.

| Quantum emitter | Wavelength | Temperature | Clock rate | Count rate | $g^{(2)}(0)$ | $\tau_r$ | $\mathcal{V}$ | Ref. |
|---|---|---|---|---|---|---|---|---|
| | nm | K | MHz | MHz | | ns | | |
| (InGa)As/GaAs QD | 920 | 4.2 | 76 [a] | 17 [b] | 0.021 | 0.048 [c] | 97.5% | [18] |
| InAs/InP QD | 1533 | 4 | 80 [a] | | 0.005 | 0.34 | 35% | [82] |
| $CsPbBr_3$ colloidal nanocrystal | 531 | 3.9 | 80 | | 0.019 | 0.23 | 56% | [48] |
| DBT in anthracene | 783.5 | 3 | 25 | 0.052 | 0.008 | 4.0 | 78% | [83] |
| DBT in anthracene | 785 | 300 | 80 | 0.5 | 0.02 [d] | 3.6 | | [84] |
| SiV in diamond | 739 | 300 | 1 | 0.0037 | 0.04 | $3 \pm 2$ [e] | | [85] |
| Color center in hBN | 436 | 4 | 80 | 0.0012 | 0.14 | 1.9 | 56% | [86] |
| Color center in hBN | 645 | 300 | 40 | 0.51 | 0.08 [f] | 3.9 | | [87] |
| $WSe_2$ 2D material | 807.3 | 4.2 | 5 | 0.067 | 0.17 | ≈ 100 [g] | | [88] |

[a] $\pi$-pulse excitation; [b] The actual count rate was 1.7 MHz, but this was measured after attenuating the photon stream by a factor of 9.9 to prevent detector saturation; [c] Purcell enhanced; [d] Measured at 40 MHz; [e] The accepted value is around 1.7 ns. See, for example,[89]; [f] Measured at 10 MHz; [g] Estimated by the author from the published HBT data.

the size of the QD and the strain within it, both of which can be controlled to some extent by the growth conditions. In this way, it has been possible to extend the wavelength to the telecom O-band around 1300 nm,[95,96] and a plug&play quantum key distribution (QKD) testbed has been developed.[97] However, the strain energy due to the lattice constant mismatch builds up as the QDs get larger, and it is impractical to push InAs/GaAs beyond the O-band, making it necessary to follow different approaches to reach the telecom C-band around 1550 nm. One option is to use InP as the host material.[15,35,36,98,99] The lattice-mismatch between InAs

and InP is smaller than with GaAs, and so larger QDs can form, leading to longer emission wavelengths. Another possibility is to deposit a metamorphic InGaAs layer on top of a GaAs substrate and grow the QDs on InGaAs rather than on GaAs, again to reduce the strain.[37,38] In this way, single-photon distribution in a metropolitan fibre network using QD sources operating at the C-band has been demonstrated[100] as well as QKD over a 79 km fibre link.[101] The second row in Table 2 gives representative state-of-the-art performance figures for the C-band QD single-photon sources.[82] While excellent single-photon purity has been demonstrated, the raw HOM visibility remains lower than for the ≈ 900 nm QDs. Significant progress is being made to improve $\mathcal{V}$,[102] and the recent results in ref. [36] demonstrate that very high visibility can be achieved by post-selection techniques.

Shorter wavelength QDs based on the GaAs/AlGaAs system are also being developed for coupling to Rb atomic quantum memories at 780 nm. These QDs have shown excellent properties both in terms of their transform-limited linewidth[39] and photon indistinguishability.[103] The QDs can also be tuned to the SiV transition at ≈ 737 nm, allowing further possibilities for hybrid devices.[104] For still shorter wavelengths in the visible and UV range, nitride quantum dots have been developed, for example GaN/AlN and InGaN/GaN.[40,41] Since these nitride quantum dots have large confinement energies, they excitons remain stable at higher temperatures, and single-photon emission at 350 K has been reported for a GaN QD formed near the tip of a nanowire.[105]

### 3.3. Colloidal Quantum Dots

Colloidal quantum dots are now routinely used in classical photonic applications such as displays. However, their use as single-photon sources is not so well developed, despite the fact that they preceded epitaxial QDs for the observation of anti-bunching.[4] One of the issues is the problem of blinking,[106] but major progress has been made with the development of core-shell II-VI QDs, especially when the QDs are coupled to nanocavities.[107] In this way, single-photon emission over a wide range of wavelengths spanning the visible to the near infrared has been reported up to room temperature (see e.g., refs. [42, 43]), and recent work includes the integration of colloidal QDs with nanophotonic circuits.[44]

Most research on colloidal QDs focuses on II-VI materials, but other types of quantum dots are coming to the fore. InP QDs containing no heavy metals are attractive due to their lack of long-term environmental issues,[45,46] while perovskite QDs are developing rapidly.[108] For example, bright single-photon emission has been reported for a perovskite QD at room temperature,[47] and the Hong–Ou–Mandel visibility achieved in another QD was 56% at 3.9 K.[48] (See third row in Table 2.)

### 3.4. Molecular Systems

The first demonstration of quantum emission for a solid-state material was made in 1992 on a single pentacene molecule embedded within a *p*-terphenyl crystal,[2] and pulsed single-photon emission at room temperature was demonstrated as early as 2000.[109] Single-photon emission has now been observed for a wide range of molecular materials spanning the visible and near infrared spectral range.[50,51] Table 2 includes some recent results for the DBT (dibenzoterrylene) molecule in anthracene at both cryogenic and room temperatures.

In the most recent work, a photon indistinguishability of 52% has been determined at 4.7 K,[110] while molecular single-photon sources have been integrated within photonic circuits[111] and implemented in a QKD system.[84] Meanwhile, the controlled introduction of aryl defects by chemical methods has led to much progress on single-photon emission from carbon nanotubes.[52,53] The emission wavelength is in the telecom O-band range around 1300 nm, making them compatible with silicon nano-cavities and hence Purcell enhancement,[112] while recent room-temperature results demonstrate high indistinguishability at a wavelength close to the C-band.[113]

### 3.5. Color Centers

Quantum emission has been observed for a great variety of color centers. (See ref. [114] for a recent review.) These are present in most crystals, and the observation of quantum emission requires a low density of defects so that only one of them lies within the excitation area. The defects emit at photon energies within the bandgap of the host, allowing a wide range of wavelengths to be reached depending on the type of color center.

Early work focussed mainly on defects in diamond (see e.g., ref. [115]), where the nitrogen-vacancy (NV) defect emitting at 637 nm received much attention. This defect suffers from strong phonon coupling, which means that only about 3% of the photons are emitted on the zero-phonon line (ZPL), and the radiative lifetime is relatively long (≈ 30 ns). As a consequence, other types of defect have been investigated, such as the silicon-vacancy (SiV) center that emits round 738 nm and has more than 70% of its emission in the ZPL.[116] The SiV center has a shorter lifetime (≈ 2 ns) than NV, which allows higher single-photon rates,[117] and its inversion symmetry makes it relatively immune to random electrostatic fluctuations, leading to high coherence and hence high photon indistinguishability.[89]

Other centers such as the germanium vacancy (GeV) emitting around 602 nm,[58,59] the tin vacancy (SnV) at about 620 nm[63,118] and the lead vacancy (PbV) emitting at about 552 nm[61] are also showing considerable promise. Transform-limited emission has been demonstrated for some of these, with a HOM indistinguishability of 63% and quantum control demonstrated for the SnV center at 3.6 K,[119] while the PbV center is relatively robust to temperature.[120] Moreover, the use of cavities to enhance the emission via the Purcell effect has been shown to give larger ZPL fractions and shorter radiative lifetimes,[55,57,62,121] while the use of nanowires and plasmonic enhancement are also highly beneficial.[54,56,60]

The experience and understanding of color centers in diamond has burgeoned a whole field of research into quantum emitters in other wide-gap crystals such as silicon carbide (SiC), silicon nitride ($Si_3N_4$), and hexagonal boron nitride (hBN). The first two are widely used in the electronics and photonics industries

and hence have mature technologies that can produce advanced devices. SiC hosts many color centers in its various polymorphs, some of which emit at technologically important telecom wavelengths in the near infrared,[66,67] while silicon nitride has bright defects that emit in the visible spectral range.[68] hBN is a layered structure that is compatible with strain-engineered quantum emitters in 2D-materials. (See Section 3.6 below.) However, it can host color-center single-photon sources in its own right that typically emit in the visible spectral region.[69,70] A photon indistinguishability of 56% has recently been determined for a 436 nm emitter at 4 K, with a value of 90% predicted to be in reach by using Purcell enhancement, while good photon count rates with acceptable $g^{(2)}(0)$ values at room temperature have been reported at 645 nm. (See results from refs. [86] and [87] in Table 2.)

Another rapidly developing field is the study of color centers in silicon, which has obvious interest on account of the dominance of silicon in electronics and its widespread use in advanced photonics. Since the bandgap of silicon is 1.1 eV, these color centers emit at wavelengths longer than 1100 nm in spectral regions that include the telecom O- and C-bands around 1300 and 1550 nm,[64,65] and their emission can be enhanced by using optical nanocavities.[122]

### 3.6. 2D Materials

The research field of graphene-like layered 2D materials is highly active at present, with very rapid progress being made for transition-metal dichalcogenide (TMDC) monolayers following the independent observation of quantum emitters by four different research groups in 2015. (See refs. [74, 123–126] for recent reviews.) In these materials the quantum emitter is formed when excitons are trapped in quantum-dot-like potential minima caused by strain. The most widely studied materials are $WS_2$, $WSe_2$ and $MoSe_2$, with emission at near-infrared wavelengths, while $MoTe_2$ has been shown to emit down into the telecom O- and C-band range.[75] Biexciton states as in Figure 4b have been clearly identified, with cascaded single-photon emission on both the $2X \rightarrow X$ and $X \rightarrow 0$ transitions demonstrated for $WSe_2$.[127] Good $g^{(2)}(0)$ values have been achieved, and a strain-engineered $WSe_2$ source emitting at 807 nm was recently implemented in a QKD test system.[128] (See bottom row in Table 2 for performance indicators.) Meanwhile a very high first-lens brightness of 65% has been reported with $g^{(2)}(0) = 4.7\%$ by coupling the TMDC monolayer to an open cavity, although the HOM visibility was low due to the unstabilized environment.[129]

The connection between the strain potential and the quantum emitter provides a natural mechanism for strain-engineered devices. The wavelength can be tuned by varying the strain,[130] while the location of the emitter can be determined by laying the 2D material over pre-patterned substrates that create localized strain points. In this way it has been possible to demonstrate site control of the quantum emitter,[131] enabling accurate positioning relative to a cavity, thereby optimizing the coupling efficiency and hence the Purcell enhancement.[132] It has also been possible to make large arrays of quantum emitters,[133] including those of $MoTe_2$ emitting at telecom wavelengths.[134]

Hexagonal boron nitride (hBN) is rapidly emerging as a very promising material in the context of quantum emitters. (See ref. [124] for a review.) Progress on color-center quantum emitters in hBN crystals was noted in Section 3.5, but hBN is also a layered 2D material, and quantum emitters can be induced by strain just as for TMDCs. In this way, arrays of emitters have been demonstrated on patterned substrates, with $g^{(2)}(0)$ values below 0.5 at room temperature.[135,136]

### 3.7. Rare Earths

Rare-earth ions from elements 57–70 are widely used in classical photonics, for example in solid-state lasers, phosphors, and fibre-based optical amplifiers. The ions are doped into the host material, and individual quantum emitters are isolated by using low doping levels. They could be considered as a type of color center, but they differ from the ones considered in Section 3.5 on account of the 4f nature of the active electronic states. Moreover, many of the color centers considered in Section 3.5 involve vacancy-based defects, whereas the rare-earth emitters involve the deliberate introduction of dopant impurities.

The optical transitions that are used in rare-earth-ion quantum emitters take place between different angular momentum states derived from the 4f orbitals. These $f \rightarrow f$ transitions are forbidden by electric-dipole selection rules, and therefore have low probabilities with correspondingly long radiative lifetimes. The long lifetimes are advantageous for developing quantum memories, but inevitably lead to low brightness. Much of the research with these materials is therefore focused around enhancing the emission by using the Purcell effect in nano-cavities.[137,138] In this way, anti-bunching has been observed for several different ions in a variety of hosts, for example: $Nd^{3+}$ in $YVO_4$ emitting at 880 nm[76] and $Yb^{3+}$ emitting around 980 nm in $LiNbO_3$,[77] $YVO_4$,[78] and optical fibre.[79]

The $Er^{3+}$ ion is receiving considerable attention on account of its telecom-compatible transitions around 1550 nm. Purcell-enhanced anti-bunching has been observed in several wide-gap insulators such as $LiNbO_3$,[80] $CaWO_4$,[81] and YSO,[139] while a 78-fold enhancement of an $Er^{3+}$ single emitter has recently been reported in a silicon nanobeam cavity.[140]

## 4. Discussion

A major issue that holds back wide-scale deployment of solid-state quantum emitters is the operating temperature. In general, all of the solid-state quantum emitters work best at low temperatures. Indeed, the nearly ideal results for the InAs/GaAs QDs are only obtained with the sample held at liquid helium temperatures ($\approx$ 4 K), as phonon scattering degrades the performance as the temperature increases. In this context, the wide-gap GaN quantum dots are more robust to temperature,[105] and some of the color-center sources can give good results even at room temperature. (See e.g., refs. [54, 66, 68]). Hexagonal boron nitride (hBN) and colloidal QDs can also work well at room temperature (see e.g., refs. [42, 141]), although none of these room-temperature results match the performance demonstrated for the InAs QDs at cryogenic temperatures, especially as regards the photon indistinguishability.

The fact that some solid-state emitters are compatible with advanced photonic technologies and hence can be embedded within high quality-factor nano-cavities and slow-light

waveguides[142,143] could provide a route to overcoming the temperature issue. The shortening of the radiative lifetime by the Purcell effect makes the emitter less susceptible to dephasing[17] and the most recent studies suggest that this could preserve the optimal performance to higher temperatures,[144] possibly within the range of miniature cryo-coolers.[97,145] In fact, the use of the cavity is a win-win situation: it speeds up the emission, improves the collection efficiency and mitigates against decoherence. The only drawback is that it does restrict the bandwidth, but the small modal volumes that are possible mean that the Q factor does not have to be especially large to achieve usable Purcell factors. Circular Bragg grating (bullseye) cavity designs show considerable promise here, as there combine very good collection efficiency with reasonable Purcell factors over moderate bandwidths.[146,147]

The compatibility of solid-state emitters with advanced technologies has other benefits. An electrically-pumped single-photon light-emitting diode was demonstrated as early as 2002,[148] and much progress has been made since then.[149] However, electrical excitation is not ideal, as timing jitter is introduced by the process of capturing the carriers into the quantum emitter, and the large number of free charges in the device can introduce noise and dephasing. These problems can be avoided by using resonant optical excitation techniques that pump the electrons directly to the relevant excited state, thereby removing the carrier relaxation time, and also limiting the creation of unwanted charge carriers. Resonant pumping also allows on-demand operation. (See Section 2.4.)

Scalability is an issue that has to be addressed for large-scale photonic quantum computing. The great drawback of the InAs quantum-dot sources is that the QDs are formed by random epitaxial growth, which leads to inhomogeneity in their size and shape, and hence emission wavelength. Other types of sources such as diamond vacancy centers are clearly better in this respect, as the emission wavelength should be the same for all emitters. However, even these have inhomogeneity at the microscopic scale due to local environmental variations and have to be tuned to bring two emitters to exact resonance.[150]

A successful work-around for the spectral inhomogeneity of self-organized quantum dots has been developed based on demultiplexing. This exploits the fact that the QDs can emit long chains of highly indistinguishable photons,[18,33] which makes it feasible to turn a stream of single photons produced at a clock-rate of $f$ into a stream of $N$ photons at rate $f/N$. In this way, boson sampling tests with 20 photons have been performed[151] as well as measurements of multi-photon indistinguishability.[152]

Another type of inhomogeneity relates to the position of the emitter, which is also random for self-organized growth. Site-control methods can be used for quantum dots (see e.g., ref. [153]), while ion-implantation techniques can be used to position vacancy defects in diamond,[154] and strain engineering can be used for 2D materials.[73,155] In the case of the InAs QDs, much progress has been made in limiting the effects of spatial inhomogeneity by using in-situ lithography,[156,157] and 15 deterministically-fabricated single-photon sources have been bench-marked with a spread of wavelengths within the range accessible by Stark tuning.[158]

For some types of quantum emitters, the issue of stability remains pertinent. The harder inorganic materials can be very robust, and the InAs quantum dot source used in the author's laboratory for ref. [17] worked almost continuously under intense excitation for five years. However, organic materials can degrade due to oxidation, and colloidal QD sources suffer from blinking due to random surface charges. The development of core-shell colloidal QDs has greatly improved the stability,[106] but further work is still needed.

In recent years there has been much interest in integrating quantum emitters into photonic circuits.[159] The InAs quantum dots are leading the way with advanced functionality demonstrated in III–V photonic circuits (see e.g., ref. [160]) along with hybrid integration into other platforms such as $Si_3N_4$,[161] and $LiNbO_3$.[162] However, other materials (e.g., colloidal QDs,[44] single molecules,[111] TMDCs[163]) are also progressing rapidly, and the discovery of quantum emitters within the photonic platform material itself — e.g., in $Si_3N_4$, SiC and silicon: see Section 3.5 — clearly opens many opportunities.

One issue that arises when integrating the emitter into photonic circuits is the difficulty in implementing coherent pumping schemes. In these schemes the resonant or near-resonant pump laser has to be separated from the emitter's photons (see Section 2.4), and this can be particularly challenging in on-chip geometries. One successful method for in-plane resonant pumping is to couple the single photons to a different waveguide mode to the pump laser in a dual-mode device.[164,165]

As a final point, it is worth mentioning that some of the quantum emitters discussed in this perspective can trap single electrons or holes and can hence be used as spin qubits. For example, the $NV^-$ and $SiV^-$ centers in diamond have been extensively studied, but there are many other possibilities as well.[166] Some of the charged defects in hBN look especially promising,[167–170] while the discovery of single spins in silicon T-centers opens possibilities for long-lived quantum memories for telecom-wavelength photons.[65]

## 5. Conclusion

The research field of solid-state emitters has made tremendous progress in the past three decades since the first results in 1992. Table 1 shows that a wide range of wavelengths is available, opening up a great variety of applications. Compared to the rival approach based on heralded down-conversion, the great advantage of quantum emitters is that they can operate deterministically (see Section 2.4). They can also be very fast, and III-V QD sources are the best single photon-sources available at present, giving nearly ideal performance at low temperatures. The award of the 2023 Nobel Prize for Chemistry for the discovery of quantum dots raises hopes that QD single-photon sources can be commercialized. In fact, III-V QD sources are now available from several companies,[171] but these are costly systems that are only being used in research laboratories at present. Other material systems are not at the same level of maturity, but some of them are making very rapid progress.

The rapid progress in the sources means that applications in quantum photonics are becoming more widespread. A review of work done with semiconductor quantum dots in quantum communications may be found in ref. [172] and several examples of the use of solid-state quantum emitters in QKD and quantum random-number generation systems have been cited in this perspective.[84,97,100,101,128] Boson sampling tests with

as many as 20 photons from a quantum-dot source have been implemented[151] and one of the commercial companies mentioned in ref. [171] has launched a quantum-computing platform based on their devices.[94] The generation of entangled photons from solid-state quantum emitters opens further applications such as super-resolved optical phase measurements[173] and bilocality demonstrations.[174] A great deal has been achieved, but there is still much to do.

## Acknowledgements

The author would like to thank the EPSRC for current financial support via grants EP/V026496/1, EP/S030751/1 and EP/T001011/1, and for previous support over many years. The author would also like to acknowledge many discussions that have helped formulate the views expressed in this perspective with colleagues at the University of Sheffield and with co-workers around the world.

## Conflict of Interest

The authors declare no conflict of interest.

## Keywords

color center, quantum emitter, quantum dot, single-photon source, single molecule

Received: November 2, 2023
Revised: July 3, 2024
Published online:

[1] J. Kimble, M. Dagenais, L. Mandel, *Phys. Rev. Lett.* **1977**, *39*, 691.
[2] T. Basché, W. Moerner, M. Orrit, H. Talon, *Phys. Rev. Lett.* **1992**, *69*, 1516.
[3] R. Brouri, A. Beveratos, J.-P. Poizat, P. Grangier, *Opt. Lett.* **2000**, *25*, 1294.
[4] P. Michler, A. Imamoglu, M. Mason, P. Carson, G. Strouse, S. Buratto, *Nature* **2000**, *406*, 968.
[5] S. Hepp, M. Jetter, S. L. Portalupi, P. Michler, *Adv. Quantum Technol.* **2019**, *2*, 1900020.
[6] R. Trivedi, K. A. Fischer, J. Vučković, K. Müller, *Adv. Quantum Technol.* **2020**, *3*, 1900007.
[7] R. Hanbury Brown, R. Twiss, *Nature* **1956**, *177*, 27.
[8] M. Davanço, C. S. Hellberg, S. Ates, A. Badolato, K. Srinivasan, *Phys. Rev. B* **2014**, *89*, 161303.
[9] M. Fox, *Quantum Optics: an Introduction*, Oxford University Press, Oxford **2006**.
[10] L. Schweickert, K. D. Jöns, K. D. Zeuner, S. F. Covre da Silva, H. Huang, T. Lettner, M. Reindl, J. Zichi, R. Trotta, A. Rastelli, V. Zwiller, *Appl. Phys. Lett.* **2018**, *112*, 093106.
[11] C. K. Hong, Z. Y. Ou, L. Mandel, *Phys. Rev. Lett.* **1987**, *59*, 2044.
[12] A. Kuhlmann, J. Prechtel, J. Houel, A. Ludwig, D. Reuter, A. Wieck, Warburton Warburton, *Nat. Commun.* **2015**, *6*, 8204.
[13] J. C. Bienfang, T. Gerrits, P. S. Kuo, A. Migdall, S. Polyakov, O. Slattery, *NIST Internal Report 8486* **2023**, https://doi.org/10.6028/NIST.IR.8486.
[14] J.-M. Gérard, B. Sermage, B. Gayral, B. Legrand, E. Costard, V. Thierry-Mieg, *Phys. Rev. Lett.* **1998**, *81*, 1110.
[15] A. Musiał, P. Holewa, P. Wyborski, M. Syperek, A. Kors, J. Reithmaier, G. Sęk, M. Benyoucef, *Adv. Quantum Technol.* **2019**, *3*, 1900082.
[16] E. Purcell, *Phys. Rev.* **1946**, *69*, 681.
[17] F. Liu, A. Brash, J. O'Hara, L. Martins, C. Phillips, R. Coles, B. Royall, E. Clarke, C. Bentham, N. Prtljaga, I. Itskevich, L. Wilson, M. Skolnick, A. Fox, *Nat. Nanotechnol.* **2018**, *13*, 835.
[18] N. Tomm, A. Javadi, N. Antoniadis, D. Najer, M. Lobl, A. Korsch, R. Schott, S. Valentin, A. Wieck, A. Ludwig, R. Warburton, *Nat. Nanotechnol.* **2021**, *16*, 399.
[19] H. Shao, G. Ying, S. Lennon, F. Brossard, J. Griffiths, L. Nuttall, V. Osokin, E. Clarke, H. He, R. Taylor, *Appl. Phys. Lett.* **2020**, *117*, 043103.
[20] F. D. Stefani, J. P. Hoogenboom, E. Barkai, *Phys. Today* **2009**, *62*, 34.
[21] W. L. Barnes, G. Björk, J. M. Gérard, P. Jonsson, J. A. E. Wasey, P. T. Worthing, V. Zwiller, *Eur. Phys. J. D* **2002**, *18*, 197.
[22] L. Bremer, C. Jimenez, S. Thiele, K. Weber, T. Huber, S. Rodt, A. Herkommer, S. Burger, S. Hofling, H. Giessen, S. Reitzenstein, *Opt. Express* **2022**, *30*, 15913.
[23] H. Wang, Y.-M. He, T. Chung, H. Hu, Y. Yu, S. Chen, X. Ding, M. Chen, J. Qin, X. Yang, R.-Z. Liu, Z. Duan, J. Li, S. Gerhardt, K. Winkler, J. Jurkat, L.-J. Wang, N. Gregersen, Y.-H. Huo, Q. Dai, S. Yu, S. Höfling, C.-Y. Lu, J.-W. Pan, *Nat. Photonics* **2019**, *13*, 770.
[24] J. H. Quilter, A. J. Brash, F. Liu, M. Glässl, A. M. Barth, V. M. Axt, A. J. Ramsay, M. S. Skolnick, A. M. Fox, *Phys. Rev. Lett.* **2015**, *114*, 137401.
[25] K. H. Madsen, S. Ates, J. Liu, A. Javadi, S. M. Albrecht, I. Yeo, S. Stobbe, P. Lodahl, *Phys. Rev. B* **2014**, *90*, 155303.
[26] Y.-M. He, H. Wang, C. Wang, M. C. Chen, X. Ding, J. Qin, Z. C. Duan, S. Chen, J. P. Li, R.-Z. Liu, C. Schneider, M. Atatüre, S. Höfling, C.-Y. Lu, J.-W. Pan, *Nat. Phys.* **2019**, *15*, 941.
[27] Y. Karli, F. Kappe, V. Remesh, T. K. Bracht, J. Munzberg, S. Covre da Silva, T. Seidelmann, V. M. Axt, A. Rastelli, D. E. Reiter, G. Weihs, *Nano Lett.* **2022**, *22*, 6567.
[28] G. Zhang, Y. Cheng, J.-P. Chou, A. Gali, *Appl. Phys. Rev.* **2020**, *7*, 031308.
[29] S.-K. Liao, H.-L. Yong, C. Liu, G.-L. Shentu, D.-D. Li, J. Lin, H. Dai, S.-Q. Zhao, B. Li, J.-Y. Guan, W. Chen, Y.-H. Gong, Y. Li, Z.-H. Lin, G.-S. Pan, J. S. Pelc, M. M. Fejer, W.-Z. Zhang, W.-Y. Liu, J. Yin, J.-G. Ren, X.-B. Wang, Q. Zhang, C.-Z. Peng, J.-W. Pan, *Nat. Photonics* **2017**, *11*, 509.
[30] L. Hanschke, K. A. Fischer, S. Appel, D. Lukin, J. Wierzbowski, S. Sun, R. Trivedi, J. Vučković, J. J. Finley, K. Müller, *npj Quantum Inf.* **2018**, *4*, 43.
[31] Y. Arakawa, M. Holmes, *Appl. Phys. Rev.* **2020**, *7*, 021309.
[32] P. Senellart, G. Solomon, A. White, *Nat. Nanotechnol.* **2017**, *12*, 1026.
[33] R. Uppu, F. Pedersen, Y. Wang, C. Olesen, C. Papon, X. Zhou, L. Midolo, S. Scholz, A. Wieck, A. Ludwig, P. Lodahl, *Sci. Adv.* **2020**, *6*, eabc8268.
[34] H. Ollivier, I. Maillette de Buy Wenniger, S. Thomas, S. Wein, A. Harouri, G. Coppola, P. Hilaire, C. Millet, A. Lemaître, I. Sagnes, O. Krebs, L. Lanco, J. Loredo, C. Antón, N. Somaschi, P. Senellart, *ACS Photonics* **2020**, *7*, 1050.
[35] M. Anderson, T. Müller, J. Skiba-Szymanska, A. Krysa, J. Huwer, R. Stevenson, J. Heffernan, D. Ritchie, A. Shields, *Appl. Phys. Lett.* **2021**, *118*, 014003.
[36] P. Holewa, D. A. Vajner, E. Zięba-Ostój, M. Wasiluk, B. Gaál, A. Sakanas, M. Burakowski, P. Mrowiński, B. Krajnik, M. Xiong, K. Yvind, N. Gregersen, A. Musiał, A. Huck, T. Heindel, M. Syperek, E. Semenova, *Nat. Commun.* **2024**, *15*, 3358.
[37] S. Portalupi, M. Jetter, P. Michler, *Semicond. Sci. Technol.* **2019**, *34*, 053001.
[38] C. Nawrath, H. Vural, J. Fischer, R. Schaber, S. Portalupi, M. Jetter, P. Michler, *Appl. Phys. Lett.* **2021**, *118*, 244002.

[39] L. Zhai, M. Lobl, G. Nguyen, J. Ritzmann, A. Javadi, C. Spinnler, A. Wieck, A. Ludwig, R. Warburton, *Nat. Commun.* **2020**, *11*, 4745.
[40] M. J. Holmes, T. Zhu, F. C.-P. Massabuau, J. Jarman, R. A. Oliver, Y. Arakawa, *APL Mater.* **2021**, *9*, 061106.
[41] J. Stachurski, S. Tamariz, G. Callsen, R. Butte, N. Grandjean, *Light Sci Appl* **2022**, *11*, 114.
[42] X. Lin, X. Dai, C. Pu, Y. Deng, Y. Niu, L. Tong, W. Fang, Y. Jin, X. Peng, *Nat. Commun.* **2017**, *8*, 1132.
[43] S. Feng, C. Cheng, C. Wei, J. Yang, Y. Chen, Y. Chuang, Y. Fan, C. Chuu, *Phys. Rev. Lett.* **2017**, *119*, 143601.
[44] A. Eich, T. Spiekermann, H. Gehring, L. Sommer, J. Bankwitz, P. Schrinner, J. Preuß, S. Michaelis de Vasconcellos, R. Bratschitsch, W. Pernice, C. Schuck, *ACS Photonics* **2022**, *9*, 551.
[45] A. H. Proppe, D. B. Berkinsky, H. Zhu, T. Sverko, A. E. K. Kaplan, J. R. Horowitz, T. Kim, H. Chung, S. Jun, M. G. Bawendi, *Nat. Nanotechnol.* **2023**, *18*, 993.
[46] G. Almeida, R. F. Ubbink, M. Stam, I. du Fossé, A. J. Houtepen, *Nat. Rev. Mater.* **2023**, *8*, 742.
[47] C. Zhu, M. Marczak, L. Feld, S. C. Boehme, C. Bernasconi, A. Moskalenko, I. Cherniukh, D. Dirin, M. I. Bodnarchuk, M. V. Kovalenko, G. Raino, *Nano Lett.* **2022**, *22*, 3751.
[48] A. E. K. Kaplan, C. J. Krajewska, A. H. Proppe, W. Sun, T. Sverko, D. B. Berkinsky, H. Utzat, M. G. Bawendi, *Nat. Photonics* **2023**, *17*, 775.
[49] M. Rezai, J. Wrachtrup, I. Gerhardt, *Phys. Rev. X* **2018**, *8*, 031026.
[50] C. Toninelli, I. Gerhardt, A. Clark, A. Reserbat-Plantey, S. Gotzinger, Z. Ristanovic, M. Colautti, P. Lombardi, K. Major, I. Deperasinska, W. Pernice, F. Koppens, B. Kozankiewicz, A. Gourdon, V. Sandoghdar, M. Orrit, *Nat. Mater.* **2021**, *20*, 1615.
[51] M. B. Gaither-Ganim, S. A. Newlon, M. G. Anderson, B. Lee, *Oxford Open Mater. Sci.* **2022**, *3*, itac017.
[52] X. He, H. Htoon, S. K. Doorn, W. H. P. Pernice, F. Pyatkov, R. Krupke, A. Jeantet, Y. Chassagneux, C. Voisin, *Nat. Mater.* **2018**, *17*, 663.
[53] A. Saha, B. J. Gifford, X. He, G. Ao, M. Zheng, H. Kataura, H. Htoon, S. Kilina, S. Tretiak, S. K. Doorn, *Nat. Chem.* **2018**, *10*, 1089.
[54] S. Bogdanov, M. Shalaginov, A. Lagutchev, C. Chiang, D. Shah, A. Baburin, I. Ryzhikov, I. Rodionov, A. Kildishev, A. Boltasseva, V. Shalaev, *Nano Lett.* **2018**, *18*, 4837.
[55] D. Riedel, I. Söllner, B. Shields, S. Starosielec, P. Appel, E. Neu, P. Maletinsky, R. Warburton, *Phys. Rev. X* **2017**, *7*, 031040.
[56] L. Marseglia, K. Saha, A. Ajoy, T. Schroder, D. Englund, F. Jelezko, R. Walsworth, J. L. Pacheco, D. L. Perry, E. Bielejec, P. Cappellaro, *Opt. Express* **2018**, *26*, 80.
[57] E. N. Knall, C. M. Knaut, R. Bekenstein, D. R. Assumpcao, P. L. Stroganov, W. Gong, Y. Q. Huan, P. J. Stas, B. Machielse, M. Chalupnik, D. Levonian, A. Suleymanzade, R. Riedinger, H. Park, M. Loncar, M. K. Bhaskar, M. D. Lukin, *Phys. Rev. Lett.* **2022**, *129*, 053603.
[58] T. Iwasaki, F. Ishibashi, Y. Miyamoto, Y. Doi, S. Kobayashi, T. Miyazaki, K. Tahara, K. Jahnke, L. Rogers, B. Naydenov, F. Jelezko, S. Yamasaki, S. Nagamachi, T. Inubushi, N. Mizuochi, M. Hatano, *Sci. Rep.* **2015**, *5*, 12882.
[59] D. Chen, Z. Mu, Y. Zhou, J. Froch, A. Rasmit, C. Diederichs, N. Zheludev, I. Aharonovich, W. Gao, *Phys. Rev. Lett.* **2019**, *123*, 033602.
[60] H. Siampour, S. Kumar, V. Davydov, L. Kulikova, V. Agafonov, S. Bozhevolnyi, *Light: Sci. Appl.* **2018**, *7*, 61.
[61] S. Ditalia Tchernij, T. Lühmann, T. Herzig, J. Küpper, A. Damin, S. Santonocito, M. Signorile, P. Traina, E. Moreva, F. Celegato, S. Pezzagna, I. P. Degiovanni, P. Olivero, M. Jakšic`, J. Meijer, P. M. Genovese, J. Forneris, *ACS Photonics* **2018**, *5*, 4864.
[62] A. Rugar, S. Aghaeimeibodi, D. Riedel, C. Dory, H. Lu, P. McQuade, Z.-X. Shen, N. Melosh, J. Vučković, *Phys. Rev. X* **2021**, *11*, 031021.
[63] M. Trusheim, B. Pingault, N. Wan, M. Gundogan, L. De Santis, R. Debroux, D. Gangloff, C. Purser, K. Chen, M. Walsh, J. Rose, J. Becker, B. Lienhard, E. Bersin, I. Paradeisanos, G. Wang, D. Lyzwa, A. Montblanch, G. Malladi, H. Bakhru, A. Ferrari, I. Walmsley, M. Atature, D. Englund, *Phys. Rev. Lett.* **2020**, *124*, 023602.
[64] A. Durand, Y. Baron, W. Redjem, T. Herzig, A. Benali, S. Pezzagna, J. Meijer, A. Kuznetsov, J.-M. Gérard, I. Robert-Philip, M. Abbarchi, V. Jacques, G. Cassabois, A. Dréau, *Phys. Rev. Lett.* **2021**, *126*, 083602.
[65] D. B. Higginbottom, A. T. K. Kurkjian, C. Chartrand, M. Kazemi, N. A. Brunelle, E. R. MacQuarrie, J. R. Klein, N. R. Lee-Hone, J. Stacho, M. Ruether, C. Bowness, L. Bergeron, A. DeAbreu, S. R. Harrigan, J. Kanaganayagam, D. W. Marsden, T. S. Richards, L. A. Stott, S. Roorda, K. J. Morse, M. L. W. Thewalt, S. Simmons, *Nature* **2022**, *607*, 266.
[66] J. Wang, Y. Zhou, Z. Wang, A. Rasmita, J. Yang, X. Li, H. von Bardeleben, W. Gao, *Nat. Commun.* **2018**, *9*, 4106.
[67] S. Castelletto, *Mater. Quantum Technol.* **2021**, *1*, 023001.
[68] A. Senichev, O. Martin Zachariah, S. Peana, D. Sychev, X. Xu, A. Lagutchev, A. Boltasseva, V. Shalaev, *Sci. Adv.* **2021**, *7*, eabj0627.
[69] A. Shaik, P. Palla, *Sci. Rep.* **2021**, *11*, 12285.
[70] I. Aharonovich, J. P. Tetienne, M. Toth, *Nano Lett.* **2022**, *22*, 9227.
[71] S. Kumar, M. Brotóns-Gisbert, R. Al-Khuzheyri, A. Branny, G. Ballesteros-Garcia, J. F. Sánchez-Royo, B. D. Gerardot, *Optica* **2016**, *3*, 882.
[72] M. Kianinia, Z.-Q. Xu, M. Toth, I. Aharonovich, *Appl. Phys. Rev.* **2022**, *9*, 011306.
[73] M. Turunen, M. Brotons-Gisbert, Y. Dai, Y. Wang, E. Scerri, C. Bonato, K. Jöns, Z. Sun, B. Gerardot, *Nat. Rev. Phys.* **2022**, *4*, 219.
[74] S. Azzam, K. Parto, G. Moody, *Appl. Phys. Lett.* **2021**, *118*, 240502.
[75] H. Zhao, M. T. Pettes, Y. Zheng, H. Htoon, *Nat. Commun.* **2021**, *12*, 6753.
[76] T. Zhong, J. Kindem, J. Bartholomew, J. Rochman, I. Craiciu, V. Verma, S. Nam, F. Marsili, M. Shaw, A. Beyer, A. Faraon, *Phys. Rev. Lett.* **2018**, *121*, 183603.
[77] K. Xia, F. Sardi, C. Sauerzapf, T. Kornher, H.-W. Becker, Z. Kis, L. Kovacs, D. Dertli, J. Foglszinger, R. Kolesov, J. Wrachtrup, *Optica* **2022**, *9*, 445.
[78] C.-J. Wu, D. Riedel, A. Ruskuc, D. Zhong, H. Kwon, A. Faraon, *Phys. Rev. Applied* **2023**, *20*, 044018.
[79] M. Takezawa, R. Suzuki, J. Takahashi, K. Shimizu, A. Naruki, K. Katsumata, K. Nemoto, M. Sadgrove, K. Sanaka, *Phys. Rev. Applied* **2023**, *20*, 044038.
[80] L. Yang, S. Wang, M. Shen, J. Xie, H. X. Tang, *Nat. Commun.* **2023**, *14*, 1718.
[81] S. Ourari, L. Dusanowski, S. P. Horvath, M. T. Uysal, C. M. Phenicie, P. Stevenson, M. Raha, S. Chen, R. J. Cava, N. P. de Leon, J. D. Thompson, *Nature* **2023**, *620*, 977.
[82] D. A. Vajner, P. Holewa, E. Zięba-Ostój, M. Wasiluk, M. von Helversen, A. Sakanas, A. Huck, K. Yvind, N. Gregersen, A. Musiał, M. Syperek, E. Semenova, T. Heindel, *ACS Photonics* **2024**, *11*, 339.
[83] P. Lombardi, M. Colautti, R. Duquennoy, G. Murtaza, P. Majumder, C. Toninelli, *Appl. Phys. Lett.* **2021**, *118*, 204002.
[84] G. Murtaza, M. Colautti, M. Hilke, P. Lombardi, F. S. Cataliotti, A. Zavatta, D. Bacco, C. Toninelli, *Opt. Express* **2023**, *31*, 9437.
[85] M. Leifgen, T. Schröder, F. Gädeke, R. Riemann, V. Métillon, E. Neu, C. Hepp, C. Arend, C. Becher, K. Lauritsen, O. Benson, *New J. Phys.* **2014**, *16*, 023021.
[86] C. Fournier, S. Roux, K. Watanabe, T. Taniguchi, S. Buil, J. Barjon, J.-P. Hermier, A. Delteil, *Phys. Rev. Applied* **2023**, *19*, L041003.
[87] A. Al-Juboori, H. Z. J. Zeng, M. A. P. Nguyen, X. Ai, A. Laucht, A. Solntsev, M. Toth, R. Malaney, I. Aharonovich, *Adv. Quantum Technol.* **2023**, *6*, 2300038.
[88] T. Gao, M. von Helversen, C. Antòn-Solanas, C. Schneider, T. Heindel, *npj 2D Mater. Appl.* **2023**, *7*, 4.
[89] A. Sipahigil, K. D. Jahnke, L. J. Rogers, T. Teraji, J. Isoya, A. S. Zibrov, F. Jelezko, M. D. Lukin, *Phys. Rev. Lett.* **2014**, *113*, 113602.

[90] T. Heindel, J.-H. Kim, N. Gregersen, A. Rastelli, S. Reitzenstein, *Adv. Opt. Photon.* **2023**, *15*, 613.
[91] L. Dusanowski, S. Kwon, C. Schneider, S. Höfling, *Phys. Rev. Lett.* **2019**, *122*, 173602.
[92] H. Wang, Z. Duan, Y. Li, S. Chen, J. Li, Y. He, M. Chen, Y. He, X. Ding, C. Peng, C. Schneider, M. Kamp, S. Höfling, C. Lu, J. Pan, *Phys. Rev. Lett.* **2016**, *116*, 213601.
[93] C. Arnold, V. Loo, A. Lemaître, I. Sagnes, O. Krebs, P. Voisin, P. Senellart, L. Lanco, *Phys. Rev. X* **2014**, *4*, 021004.
[94] N. Maring, A. Fyrillas, M. Pont, E. Ivanov, P. Stepanov, W. Margaria, Nicoand Hease, A. Pishchagin, A. Lemaître, I. Sagnes, T. H. Au, S. Boissier, E. Bertasi, A. Baert, M. Valdivia, M. Billard, O. Acar, A. Brieussel, R. Mezher, S. C. Wein, A. Salavrakos, P. Sinnott, D. A. Fioretto, P.-E. Emeriau, N. Belabas, S. Mansfield, P. Senellart, J. Senellart, N. Somaschi, *Nat. Photonics* **2024**, *18*, 603.
[95] A. Barbiero, J. Huwer, J. Skiba-Szymanska, D. J. P. Ellis, R. M. Stevenson, T. Müller, G. Shooter, L. E. Goff, D. A. Ritchie, A. J. Shields, *ACS Photonics* **2022**, *9*, 3060.
[96] S.-W. Xu, Y.-M. Wei, R.-B. Su, X.-S. Li, P.-N. Huang, S.-F. Liu, X.-Y. Huang, Y. Yu, J. Liu, X.-H. Wang, *Photonics Res.* **2022**, *10*, B1.
[97] T. Gao, L. Rickert, F. Urban, J. Große, N. Srocka, S. Rodt, A. Musiał, K. Żołnacz, P. Mergo, K. Dybka, W. Urbańczyk, G. Sęk, S. Burger, S. Reitzenstein, T. Heindel, *Appl. Phys. Rev.* **2022**, *9*, 011412.
[98] E. M. Sala, M. Godsland, Y. I. Na, A. Trapalis, J. Heffernan, *Nanotechnology* **2021**, *33*, 065601.
[99] C. L. Phillips, A. J. Brash, M. Godsland, N. J. Martin, A. Foster, A. Tomlinson, R. Dost, N. Babazadeh, E. M. Sala, L. Wilson, J. Heffernan, M. S. Skolnick, A. M. Fox, *Sci. Rep.* **2024**, *14*, 4450.
[100] S. Gyger, K. D. Zeuner, T. Lettner, S. Bensoussan, M. Carlnäs, L. Eke mar, L. Schweickert, C. R. Hedlund, M. Hammar, T. Nilsson, J. Almlöf, S. Steinhauer, G. V. Llosera, V. Zwiller, *Appl. Phys. Lett.* **2022**, *121*, 194003.
[101] J. Yang, Z. Jiang, F. Benthin, J. Hanel, T. Fandrich, R. Joos, S. Bauer, S. Kolatschek, A. Hreibi, E. P. Rugeramigabo, M. Jetter, S. L. Portalupi, M. Zopf, P. Michler, S. Kück, F. Ding, *Light: Sci. Appl.* **2024**, *13*, 150.
[102] R. Joos, S. Bauer, C. Rupp, S. Kolatschek, W. Fischer, C. Nawrath, P. Vijayan, R. Sittig, M. Jetter, S. L. Portalupi, P. Michler, *Nano Lett.* **2024**, *24*, 8626.
[103] L. Zhai, G. N. Nguyen, C. Spinnler, J. Ritzmann, M. C. Löbl, A. D. Wieck, A. Ludwig, A. Javadi, R. J. Warburton, *Nat. Nanotechnol.* **2022**, *17*, 829.
[104] X. Cao, J. Yang, T. Fandrich, Y. Zhang, E. P. Rugeramigabo, B. Brechtken, R. J. Haug, M. Zopf, F. Ding, *Nano Lett.* **2023**, *23*, 6109.
[105] M. J. Holmes, S. Kako, K. Choi, M. Arita, Y. Arakawa, *ACS Photonics* **2016**, *3*, 543.
[106] A. L. Efros, D. J. Nesbitt, *Nat. Neurosci.* **2016**, *11*, 661.
[107] Z. Wang, J. Tang, J. Han, J. Xia, T. Ma, X.-W. Chen, *Nano Lett.* **2024**, *24*, 1761.
[108] S. Castelletto, F. De Angelis, A. Boretti, *Appl. Mater. Today* **2022**, *26*, 101401.
[109] B. Lounis, W. E. Moerner, *Nature* **2000**, *407*, 491.
[110] R. C. Schofield, C. Clear, R. A. Hoggarth, K. D. Major, D. P. S. McCutcheon, A. S. Clark, *Phys. Rev. Research* **2022**, *4*, 013037.
[111] P. Ren, S. Wei, W. Liu, S. Lin, Z. Tian, T. Huang, J. Tang, Y. Shi, X. W. Chen, *Nat. Commun.* **2022**, *13*, 3982.
[112] A. Ishii, X. He, N. F. Hartmann, H. Machiya, H. Htoon, S. K. Doorn, Y. K. Kato, *Nano Lett.* **2018**, *18*, 3873.
[113] L. Husel, J. Trapp, J. Scherzer, X. Wu, P. Wang, J. Fortner, M. Nutz, T. Hümmer, B. Polovnikov, M. Förg, D. Hunger, Y. Wang, A. Högele, *Nat. Commun.* **2024**, *15*, 3989.
[114] G. Andrini, F. Amanti, F. Armani, V. Bellani, V. Bonaiuto, S. Cammarata, M. Campostrini, T. H. Dao, F. De Matteis, V. Demontis, G. Di Giuseppe, S. Ditalia Tchernij, S. Donati, A. Fontana, J. Forneris, R. Francini, L. Frontini, R. Gunnella, S. Iadanza, A. E. Kaplan, C. Lacava, V. Liberali, F. Marzioni, E. Nieto Hernéndez, E. Pedreschi, P. Piergentili, D. Prete, P. Prosposito, V. Rigato, C. Roncolato, et al., *Photonics* **2024**, *11*, 188.
[115] S. Pezzagna, D. Rogalla, D. Wildanger, J. Meijer, A. Zaitsev, *New J. Phys.* **2011**, *13*, 035024.
[116] E. Neu, M. Agio, C. Becher, *Opt. Express* **2012**, *20*, 19956.
[117] M. Leifgen, T. Schröder, F. Gädeke, R. Riemann, V. Métillon, E. Neu, C. Hepp, C. Arend, C. Becher, K. Lauritsen, O. Benson, *New J. Phys.* **2014**, *16*, 023021.
[118] T. Iwasaki, Y. Miyamoto, T. Taniguchi, P. Siyushev, M. H. Metsch, F. Jelezko, M. Hatano, *Phys Rev Lett* **2017**, *119*, 253601.
[119] J. Arjona Martinez, R. A. Parker, K. C. Chen, C. M. Purser, L. Li, C. P. Michaels, A. M. Stramma, R. Debroux, I. B. Harris, M. Hayhurst Appel, E. C. Nichols, M. E. Trusheim, D. A. Gangloff, D. Englund, M. Atature, *Phys. Rev. Lett.* **2022**, *129*, 173603.
[120] P. Wang, L. Kazak, K. Senkalla, P. Siyushev, R. Abe, T. Taniguchi, S. Onoda, H. Kato, T. Makino, M. Hatano, F. Jelezko, T. Iwasaki, *Phys. Rev. Lett.* **2024**, *132*, 073601.
[121] E. Janitz, M. Bhaskar, L. Childress, *Optica* **2020**, *7*, 1232.
[122] V. Saggio, C. Errando-Herranz, S. Gyger, C. Panuski, M. Prabhu, L. De Santis, I. Christen, D. Ornelas-Huerta, H. Raniwala, C. Gerlach, M. Colangelo, D. Englund, *Nat. Commun.* **2024**, *15*, 5296.
[123] M. Turunen, M. Brotons-Gisbert, Y. Dai, Y. Wang, E. Scerri, C. Bonato, K. D. Jöns, Z. Sun, B. D. Gerardot, *Nat. Rev. Phys.* **2022**, *4*, 219.
[124] M. Kianinia, Z.-Q. Xu, M. Toth, I. Aharonovich, *Appl. Phys. Rev.* **2022**, *9*, 011306.
[125] S. Michaelis de Vasconcellos, D. Wigger, U. Wurstbauer, A. W. Holleitner, R. Bratschitsch, T. Kuhn, *Physica Status Solidi (b)* **2022**, *259*, 2100566.
[126] A. R.-P. Montblanch, M. Barbone, I. Aharonovich, M. Atatüre, A. C. Ferrari, *Nat. Nanotechnol.* **2023**, *18*, 555.
[127] Y.-M. He, O. Iff, N. Lundt, V. Baumann, M. Davanco, K. Srinivasan, S. Höfling, C. Schneider, *Nat. Commun.* **2016**, *7*, 13409.
[128] T. Gao, M. von Helversen, C. Antón-Solanas, C. Schneider, T. Heindel, *npj 2D Mater. Appl.* **2023**, *7*, 4.
[129] J. C. Drawer, V. N. Mitryakhin, H. Shan, S. Stephan, M. Gittinger, L. Lackner, B. Han, G. Leibeling, F. Eilenberger, R. Banerjee, S. Tongay, K. Watanabe, T. Taniguchi, C. Lienau, M. Silies, C. Anton-Solanas, M. Esmann, C. Schneider, *Nano Lett.* **2023**, *23*, 8683.
[130] O. Iff, D. Tedeschi, J. Martín-Sánchez, M. Moczała-Dusanowska, S. Tongay, K. Yumigeta, J. Taboada-Gutiérrez, M. Savaresi, A. Rastelli, P. Alonso-González, S. Höfling, R. Trotta, C. Schneider, *Nano Lett.* **2019**, *19*, 6931.
[131] S. Kumar, A. Kaczmarczyk, B. D. Gerardot, *Nano Lett.* **2015**, *15*, 7567.
[132] O. Iff, Q. Buchinger, M. Moczała-Dusanowska, M. Kamp, S. Betzold, M. Davanco, K. Srinivasan, S. Tongay, C. Antón-Solanas, S. Höfling, C. Schneider, *Nano Lett.* **2021**, *21*, 4715.
[133] C. Palacios-Berraquero, D. M. Kara, A. R.-P. Montblanch, M. Barbone, P. Latawiec, D. Yoon, A. K. Ott, M. Loncar, A. C. Ferrari, M. Atatüre, *Nat. Commun.* **2017**, *8*, 15093.
[134] H. Zhao, M. T. Pettes, Y. Zheng, H. Htoon, *Nat. Commun.* **2021**, *12*, 6753.
[135] C. Li, N. Mendelson, R. Ritika, Y. Chen, Z.-Q. Xu, M. Toth, I. Aharonovich, *Nano Lett.* **2021**, *21*, 3626.
[136] J. C. Stewart, Y. Fan, J. S. H. Danial, A. Goetz, A. S. Prasad, O. J. Burton, J. A. Alexander-Webber, S. F. Lee, S. M. Skoff, V. Babenko, S. Hofmann, *ACS Nano* **2021**, *15*, 13591.
[137] T. Zhong, P. Goldner, *J. Nanophotonics* **2019**, *8*, 2003.
[138] R. M. Pettit, F. H. Farshi, S. E. Sullivan, A. Véliz-Osorio, M. K. Singh, *Appl. Phys. Rev.* **2023**, *10*, 031307.
[139] A. Ulanowski, B. Merkel, A. Reiserer, *Sci. Adv.* **2022**, *8*, eabo4538.
[140] A. Gritsch, A. Ulanowski, A. Reiserer, *Optica* **2023**, *10*, 783.

[141] G. Grosso, H. Moon, B. Lienhard, S. Ali, D. Efetov, M. Furchi, P. Jarillo-Herrero, M. Ford, I. Aharonovich, D. Englund, *Nat. Commun.* **2017**, *8*, 705.
[142] M. Arcari, I. Söllner, A. Javadi, S. Lindskov Hansen, S. Mahmoodian, J. Liu, H. Thyrrestrup, E. H. Lee, J. D. Song, S. Stobbe, P. Lodahl, *Phys. Rev. Lett.* **2014**, *113*, 093603.
[143] H. Siampour, C. O' Rourke, A. J. Brash, M. N. Makhonin, R. Dost, D. J. Hallett, E. Clarke, P. K. Patil, M. S. Skolnick, A. M. Fox, *npj Quantum Inf.* **2023**, *9*, 15.
[144] A. J. Brash, J. Iles-Smith, *Mater. Quantum Technol.* **2023**, *3*, 045001.
[145] A. Schlehahn, L. Krüger, M. Gschrey, J. H. Schulze, S. Rodt, A. Strittmatter, T. Heindel, S. Reitzenstein, *Rev. Sci. Instrum.* **2015**, *86*, 013113.
[146] H. Wang, Y.-M. He, T. H. Chung, H. Hu, Y. Yu, S. Chen, X. Ding, M. C. Chen, J. Qin, X. Yang, R.-Z. Liu, Z. C. Duan, J. P. Li, S. Gerhardt, K. Winkler, J. Jurkat, L.-J. Wang, N. Gregersen, Y.-H. Huo, Q. Dai, S. Yu, S. Höfling, C.-Y. Lu, J.-W. Pan, *Nat. Photonics* **2019**, *13*, 770.
[147] R. Hekmati, J. P. Hadden, A. Mathew, S. G. Bishop, S. A. Lynch, A. J. Bennett, *Sci. Rep.* **2023**, *13*, 5316.
[148] Z. Yuan, B. Kardynal, R. Stevenson, A. Shields, C. Lobo, K. Cooper, N. Beattie, D. Ritchie, M. Pepper, *Science* **2002**, *295*, 102.
[149] Y. Lin, Y. Ye, W. Fang, *J. Semicond.* **2019**, *40*, 071904.
[150] R. E. Evans, M. K. Bhaskar, D. D. Sukachev, C. T. Nguyen, A. Sipahigil, M. J. Burek, B. Machielse, G. H. Zhang, A. S. Zibrov, E. Bielejec, H. Park, M. Loncăr, M. D. Lukin, *Science* **2018**, *362*, 662.
[151] H. Wang, J. Qin, X. Ding, M.-C. Chen, S. Chen, X. You, Y.-M. He, X. Jiang, L. You, Z. Wang, C. Schneider, J. J. Renema, S. Höfling, C.-Y. Lu, J.-W. Pan, *Phys. Rev. Lett.* **2019**, *123*, 250503.
[152] M. Pont, R. Albiero, S. E. Thomas, N. Spagnolo, F. Ceccarelli, G. Corrielli, A. Brieussel, N. Somaschi, H. Huet, A. Harouri, A. Lemaître, I. Sagnes, N. Belabas, F. Sciarrino, R. Osellame, P. Senellart, A. Crespi, *Phys. Rev. X* **2022**, *12*, 031033.
[153] J. Große, M. von Helversen, A. Koulas-Simos, M. Hermann, S. Reitzenstein, *APL Photonics* **2020**, *5*, 096107.
[154] C. Bradac, W. Gao, J. Forneris, M. E. Trusheim, I. Aharonovich, *Nat. Commun.* **2019**, *10*, 5625.
[155] S. Guo, S. Germanis, T. Taniguchi, K. Watanabe, F. Withers, I. J. Luxmoore, *ACS Photonics* **2023**, *10*, 2549.
[156] M. Gschrey, A. Thoma, P. Schnauber, M. Seifried, R. Schmidt, B. Wohlfeil, L. Krüger, J. H. Schulze, T. Heindel, S. Burger, F. Schmidt, A. Strittmatter, S. Rodt, S. Reitzenstein, *Nat. Commun.* **2015**, *6*, 7662.
[157] S. Rodt, S. Reitzenstein, T. Heindel, *J. Phys.: Condens. Matter* **2020**, *32*, 153003.
[158] H. Ollivier, I. Maillette de Buy Wenniger, S. Thomas, S. C. Wein, A. Harouri, G. Coppola, P. Hilaire, C. Millet, A. Lemaître, I. Sagnes, O. Krebs, L. Lanco, J. C. Loredo, C. Antón, N. Somaschi, P. Senellart, *ACS Photonics* **2020**, *7*, 1050.
[159] M. Sartison, O. Camacho Ibarra, I. Caltzidis, D. Reuter, K. D. Jöns, *Mater. Quantum Technol.* **2022**, *2*, 023002.
[160] D. D. Buhler, M. Weiss, A. Crespo-Poveda, E. D. S. Nysten, J. J. Finley, K. Muller, P. V. Santos, J. de Lima, M. M., H. J. Krenner, *Nat. Commun.* **2022**, *13*, 6998.
[161] A. Chanana, H. Larocque, R. Moreira, J. Carolan, B. Guha, E. G. Melo, V. Anant, J. Song, D. Englund, D. J. Blumenthal, K. Srinivasan, M. Davanco, *Nat. Commun.* **2022**, *13*, 7693.
[162] S. Aghaeimeibodi, B. Desiatov, J.-H. Kim, C.-M. Lee, M. A. Buyukkaya, A. Karasahin, C. J. K. Richardson, R. P. Leavitt, M. Loncăr, E. Waks, *Appl. Phys. Lett.* **2018**, *113*, 221102.
[163] K. Parto, S. I. Azzam, N. Lewis, S. D. Patel, S. Umezawa, K. Watanabe, T. Taniguchi, G. Moody, *Nano Lett* **2022**, *22*, 9748.
[164] R. Uppu, H. T. Eriksen, H. Thyrrestrup, A. D. Ugurlu, Y. Wang, S. Scholz, A. D. Wieck, A. Ludwig, M. C. Lobl, R. J. Warburton, P. Lodahl, L. Midolo, *Nat. Commun.* **2020**, *11*, 3782.
[165] X. Zhou, P. Lodahl, L. Midolo, *Quantum Science and Technology* **2022**, *7*, 025023.
[166] D. D. Awschalom, R. Hanson, J. Wrachtrup, B. B. Zhou, *Nat. Photonics* **2018**, *12*, 516.
[167] H. L. Stern, Q. Gu, J. Jarman, S. Eizagirre Barker, N. Mendelson, D. Chugh, S. Schott, H. H. Tan, H. Sirringhaus, I. Aharonovich, M. Atature, *Nat. Commun.* **2022**, *13*, 618.
[168] R. Rizzato, M. Schalk, S. Mohr, J. C. Hermann, J. P. Leibold, F. Bruckmaier, G. Salvitti, C. Qian, P. Ji, G. V. Astakhov, U. Kentsch, M. Helm, A. V. Stier, J. J. Finley, D. B. Bucher, *Nat. Commun.* **2023**, *14*, 5089.
[169] A. J. Ramsay, R. Hekmati, C. J. Patrickson, S. Baber, D. R. M. Arvidsson-Shukur, A. J. Bennett, I. J. Luxmoore, *Nat. Commun.* **2023**, *14*, 461.
[170] N. J. Guo, S. Li, W. Liu, Y. Z. Yang, X. D. Zeng, S. Yu, Y. Meng, Z. P. Li, Z. A. Wang, L. K. Xie, R. C. Ge, J. F. Wang, Q. Li, J. S. Xu, Y. T. Wang, J. S. Tang, A. Gali, C. F. Li, G. C. Guo, *Nat. Commun.* **2023**, *14*, 2893.
[171] See, for example: Quandela (quandela.com), Aegiq (aegiq.com) or Sparrow Quantum (sparrowquantum.com).
[172] D. A. Vajner, L. Rickert, T. Gao, K. Kaymazlar, T. Heindel, *Adv. Quantum Technol.* **2022**, *5*, 2100116.
[173] G. Peniakov, Z. E. Su, A. Beck, D. Cogan, O. Amar, D. Gershoni, *Phys. Rev. B* **2020**, *101*, 245406.
[174] G. Carvacho, E. Roccia, M. Valeri, F. B. Basset, D. Poderini, C. Pardo, E. Polino, L. Carosini, M. B. Rota, J. Neuwirth, S. F. Covre da Silva, A. Rastelli, N. Spagnolo, R. Chaves, R. Trotta, F. Sciarrino, *Optica* **2022**, *9*, 572.

**A. Mark Fox** is Professor of Optical Physics at the University of Sheffield. He has more than 250 publications covering a wide range of topics in semiconductor photonics and quantum optics. In recent years he has been focussing his research on III-V semiconductor quantum dots, with a special interest in their application in quantum technologies. He is the author of Optical Properties of Solids and Quantum Optics: an Introduction, both published in the Oxford Masters Series in Physics.